ACS APPLIED MATERIALS & INTERFACES

Research Article

www.acsami.org

Enhanced Electrochemical Performance of $FeWO_4$ by Coating Nitrogen-Doped Carbon

Chen Gong,[†] Yu-Jun Bai,*[,†,‡] Jun Feng,[†] Rui Tang,[†] Yong-Xin Qi,[†] Ning Lun,[†] and Run-Hua Fan*[,†]

[†]Key Laboratory for Liquid−Solid Structural Evolution and Processing of Materials (Ministry of Education), Shandong University, Jinan 250061, People's Republic of China

[‡]State Key Laboratory of Crystal Materials, Shandong University, Jinan, 250100, People's Republic of China

Supporting Information

ABSTRACT: $FeWO_4$ (FWO) nanocrystals were prepared at 180 °C by a simple hydrothermal method, and carbon-coated FWO (FWO/C) was obtained at 550 °C using pyrrole as a carbon source. The FWO/C obtained from the product hydrothermally treated for 5 h exhibits reversible capacities of 771.6, 743.8, 670.6, 532.6, 342.2, and 184.0 mAh g^{-1} at the current densities of 100, 200, 400, 800, 1600, and 3200 mA g^{-1}, respectively, whereas that from the product treated for 0.5 h achieves a reversible capacity of 205.9 mAh g^{-1} after cycling 200 times at a current density of 800 mA g^{-1}. The excellent electrochemical performance of the FWO/C results from the combination of the nanocrystals with good electron transport performance and the nitrogen-doped carbon coating.

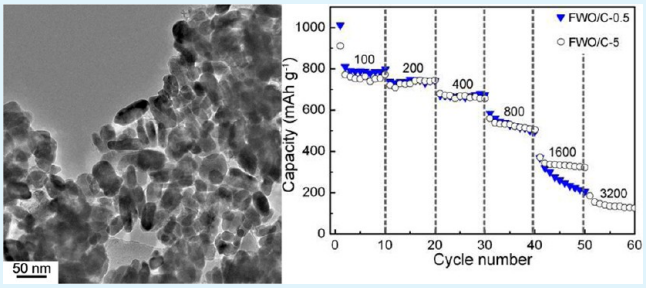

KEYWORDS: *cyclic performance, rate capability, hydrothermal treatment, impedance, N-doping, tungstate*

1. INTRODUCTION

Metal tungstates have some unique properties, such as photoluminescence,[1] catalysis,[2] antiferromagnetism,[3] and reduction,[4] and thus could be used in optical, magnetic, catalytic, and reductive fields. Because of the difficulties in preparing pure $FeWO_4$ (FWO), only a few reports have so far been concerned with the material.[1−7] The synthesis methods available include solid-state reaction,[5] spray pyrolysis,[6] and a hydrothermal route,[7] among which the hydrothermal approach is an effective way to synthesize the pure FWO.

According to the literature,[8] FWO has good electron transport performance, which is very important for electrode materials. To date, only several tungstates have been suggested as electrode materials for Li-ion batteries (LIBs). Carbon-coated $ZnWO_4$ nanorods synthesized by the hydrothermal method delivered a higher capacity than the pristine ones.[9] Carbon-coated $CaWO_4$ nanocrystals prepared by a solution precipitation method exhibited a reversible capacity of 230 ± 5 mAh g^{-1} cycling at 60 mA g^{-1}.[10] To the best of our knowledge, only one report is related to the electrochemical performance of FWO as anode materials, where the FWO nanorods demonstrated a continuous decrease in capacity within 20 cycles.[11] However, no research is so far concerned with the carbon-coated FWO (FWO/C) as anode materials.

From two very recent investigations, coating nitrogen-doped carbon (N-carbon) could effectively improve the electrochemical performance of anode materials. Fe_3O_4 coated with N-carbon revealed a high capacity of 800 mAh g^{-1} at a current density of 500 mA g^{-1}.[12] $MgFe_2O_4$ encapsualted in N-carbon delivered a reversible capacity of 744.0 mAh g^{-1} after 160 cycles at a current density of 100 mA g^{-1}.[13]

In the present work, we prepared FWO nanocrystals at 180 °C by the hydrothermal route, followed by coating carbon using pyrrole as the carbon source. The FWO/C as anode materials exhibits excellent rate capabilities and outstanding long-term cycling performance (up to 200 cycles) even charging/discharging at a current density of 800 mA g^{-1}.

2. EXPERIMENTAL METHODS

2.1. Synthesis of FWO/C. All the reagents involved are analytically pure and used without further purification. In a typical process, 2.97 g of $FeCl_2{\cdot}4H_2O$ and 4.41 g of Na_2WO_4 were dissolved in 25 mL of deionized water, respectively. The $FeCl_2$ solution was then added dropwise into the Na_2WO_4 solution under magnetic stirring. After washing three times with deionized water, the product was dried at 180 °C for 5 h, which was designated as FWO-0.

The hydrothemal treatment was conducted in a similar way except that the mixed solution was subsequently heated in different autoclaves to 180 °C for 0.5, 5, and 10 h, respectively, and the dried products were denoted as FWO-0.5, FWO-5, and FWO-10.

Pyrrole was used as the carbon source to form the carbon coating on FWO in stainless steel autoclaves. The autoclaves containing 1.5 g of FWO and 0.51 mL of pyrrole were sealed and heated to 550 °C for 5 h, and the products are correspondingly assigned to FWO/C-0, FWO/C-0.5, FWO/C-5, and FWO/C-10.

Received: January 29, 2013
Accepted: April 29, 2013
Published: April 29, 2013

   dx.doi.org/10.1021/am400392t | ACS Appl. Mater. Interfaces 2013, 5, 4209−4215

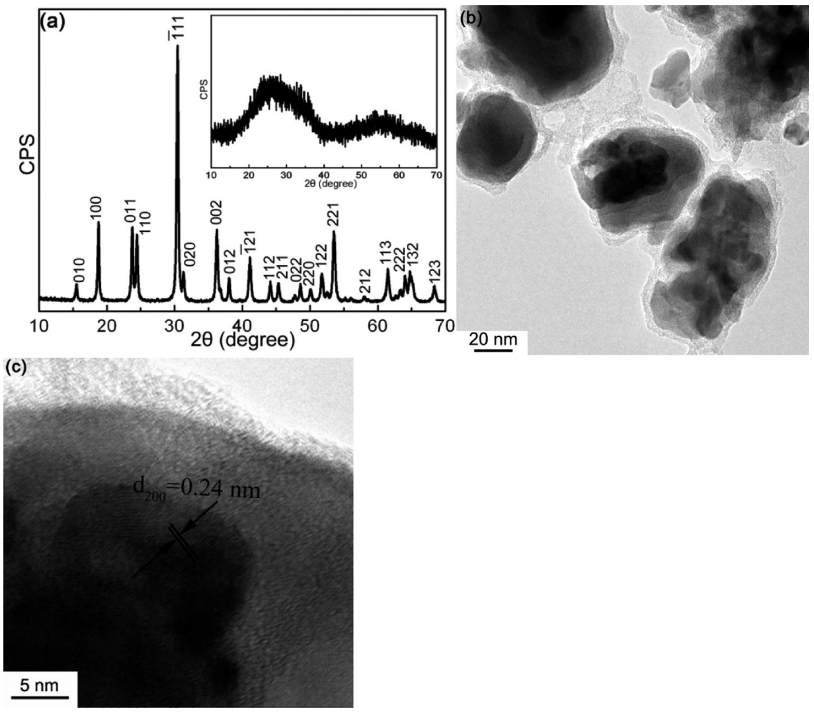

Figure 1. XRD pattern (a) and TEM images (b, c) of FWO/C-0. The inset in (a) is the XRD pattern of FWO-0.

In a comparative experiment, glucose was selected as the carbon precursor to form the carbon coating on FWO-5. Typically, 0.5 g of glucose was first dissolved in deionized water, and then mixed with 1.5 g of FWO powders under magnetic stirring. When the mixture was thoroughly dried at 105 °C, it was heated in sealed autoclaves to 550 °C for 5 h, and the product is designated as FWO/GC-5.

2.2. Characterization of the Products. XRD patterns were collected by a Rigaku Dmax-2500 diffractometer with Ni filtered Cu Kα radiation (V = 50 kV, I = 100 mA) at a scanning rate of 4° min^{-1}. The morphology of the products was examined using a JEOL JEM-2100 high-resolution transmission electron microscope (HRTEM). Raman spectra were collected on a Renishaw confocal Raman microspectroscopy (Renishaw Co. Ltd., Gloucestershire, U.K.) system with a laser excitation wavelength of 780 nm. TGA measurement was carried out in an SDT Q600 (TA Instruments Ltd., New Castle, DE) thermal-microbalance apparatus at a heating rate of 10 °C min^{-1} in an air atmosphere from ambient temperature to 950 °C to determine the content of carbon in the final product. A Quadrasorb SI sorption analyzer was adopted to acquire nitrogen adsorption/desorption isotherms at −196 °C with the samples being outgassed at 300 °C for 3 h under a vacuum in the degas port of the analyzer. The specific surface area was calculated by using the Brunauer−Emmett−Teller (BET) model. The content of carbon and nitrogen in the carbon-coated samples was quantitatively determined by a Vario EL III elemental analyzer (Elementar Analysensysteme GmbH, Germany).

2.3. Electrochemical Performance Evaluation. The electrochemical performance was tested in 2025 coin-type cells. FWO/C, carbon black, and polyvinylidene fluoride (PVDF) with a weight ratio of 8:1:1 were mixed in *n*-methyl pyrrolidinone (NMP) to form a uniform slurry, which was then coated onto a Cu foil substrate and subsequently dried in a vacuum oven at 120 °C for 10 h. Li foil was used as counter electrode, Celgard 2300 as separator, and the mixture of $LiPF_6$ in ethylene carbonate and dimethyl carbonate (1:1 by volume) as electrolyte. Half-cells were assembled in a glovebox filled with argon gas at room temperature. The performance of the cells was measured galvanostatically in the voltage range of 0.02−3 V at various current densities. The specific current density and capacity were determined according to the actual weight of active materials (FWO, FWO/C, and FWO/GC) on the Cu foil. Electrochemical impedance spectra were measured on a PARSTAT 2273 electrochemistry workstation with an ac signal amplitude of 5 mV in the frequency range from 100 kHz to 0.1 Hz. The data acquired were adopted to draw Nyquist plots using real part Z' as the X axis, and imaginary part Z'' as the Y axis. Cyclic voltammetry measurement was carried out on an electrochemistry workstation (PARSTAT 2273) over the potential range of 0−3 V vs Li/Li$^+$ at a scan rate of 0.1 mV s^{-1}.

3. RESULTS AND DISCUSSION

3.1. Product without Hydrothermal Treatment. *3.1.1. Structure and Morphology.* The XRD patterns of the products without hydrothermal treatment are shown in Figure 1a. Though the product of FWO-0 obtained by the direct reaction between $FeCl_2$ and Na_2WO_4 is an amorphous phase (the inset in Figure 1a), all the diffraction peaks resulting from FWO/C-0 accord well with those of monoclinic $FeWO_4$ (JCPDS 71-2391), and no other diffractions are detectable, implying that the as-obtained product is the pure $FeWO_4$. The amorphous FWO could transform into the crystalline phase during carbon coating at 550 °C. The average crystal size of FWO/C-0 is about 28.7 nm, calculated by using the Scherrer formula.

From the TEM image displayed in Figure 1b, FWO is encapsulated in carbon shells, and the inclusions are composed of nanocrystals with sizes from 14 to 43 nm. The structure indicates that the carbon coating formed around the FWO phase. In terms of the literature,[14] the crystallization of the amorphous phase is an efficient method to fabricate nanocrystals. The formation of the carbon coating is concomitant with the crystallization of the amorphous FWO in carbon shells. In Figure 1c, the lattice spacing of 0.24 nm corresponds to the interplanar spacing of the (200) plane for FWO, further verifying the well-crystallized FWO after carbon coating at 550 °C. The thickness of the carbon layer is about 2.6 nm. The carbon coating and the highly pure FWO with good electronic conductivity would be favorable to the electrochemical performance of FWO as anode materials for LIBs.

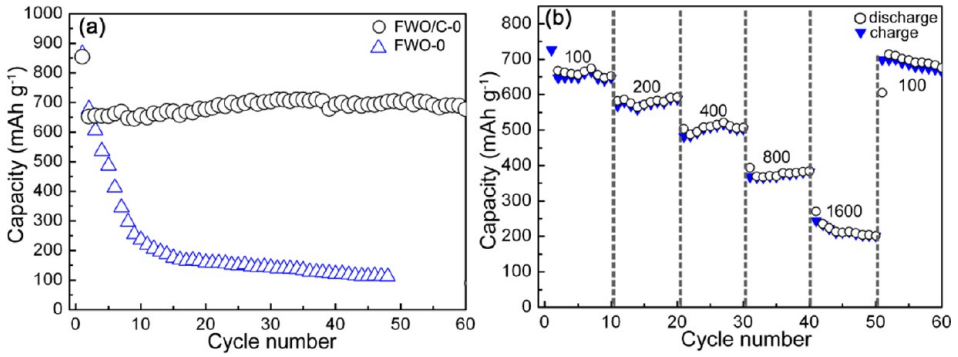

Figure 2. (a) Cyclic performance of FWO-0 and FWO/C-0 at a current density of 100 mA g^{-1}, and (b) rate capabilities of FWO/C-0.

3.1.2. Electrochemical Performance. The cyclic performance of FWO-0 and FWO/C-0 is displayed in Figure 2a, from which FWO/C-0 exhibits a reversible capacity of 676.9 mAh g^{-1} after 60 cycles, which is significantly higher than that of FWO-0 (113.3 mAh g^{-1} after 48 cycles). The enhancement confirms the beneficial effect of carbon coating on the cyclic performance of FWO. The rate capabilities of FWO/C-0 were also tested, as revealed in Figure 2b. The FWO/C-0 delivers capacities of 582.5, 487.2, 383.8, and 213.3 mAh g^{-1} (which are listed in Table 1 for comparison) when cycled every 10 times at 200, 400, 800, and 1600 mA g^{-1}, respectively, and could recover to 701.6 mAh g^{-1} during subsequent cycling at 100 mA g^{-1}. The similar phenomenon of capacity increase during cycling has also been observed in other iron oxides,[15−17] which could be ascribed to the activation of FWO/C during the first several charging/discharging cycles and the formation of polymer/gel-like films around the nanoparticles owing to the decomposition of the electrolyte. The activation is beneficial for decreasing electrochemical impedance and the formation of an SEI film for enhancing mechanical cohesion, resulting in the so-called pseudo-capacitance-type behavior.[15−17] As a consequence, good capacity retention and enhanced cyclic performance could be achieved.

Table 1. Reversible Capacities (mAh g^{-1}) of the Products at Various Current Densities (mA g^{-1})

	current density					
sample no.	100	200	400	800	1600	3200
FWO/C-0	658.9	582.5	487.2	383.8	213.3	
FWO/C-0.5	810.2	741.6	667.9	528.4	260.9	
FWO/C-5	771.6	743.8	670.6	532.6	342.2	184.0
FWO/C-10	501.2	391.6	323.7	190.7	70.7	

The Coulombic efficiency of FWO/C-0 is about 82% for the first cycle and close to 100% for the following cycles. The cycling performance of the carbon-coated FWO is much superior to that of the uncoated one in the literature.[11] As has been reported,[18,19] the uniform carbon coating could prevent the nanoparticles from agglomeration, buffer the drastic volume change of FWO nanoparticles during charging/discharging, and enhance the electronic conductivity, contributing to maintaining the reversibility of the electrochemical reactions and to preventing the capacity from fading.

Despite the excellent cyclic performance of FWO/C-0, the high-rate performance is still unsatisfactory. The possible reasons may lie in the imperfect crystallization during the preparation of FWO and the assembly of FWO nanocrystals inside the carbon shells during charging/discharging. As a result, the hydrothermal route was adopted to improve the crystallization of FWO.

3.2. Hydrothermal Products. *3.2.1. Structure and Morphology.* The XRD patterns of the products hydrothermally processed at 180 °C for 0.5 and 5 h are shown in Figure 3. The diffractions of the carbon-coated products are similar to those in Figure 1a, demonstrating the formation of FWO with high crystallization. It can be noted that the product of FWO-0.5 is partially crystallized (the inset in Figure 3a), and that of FWO-5 is thoroughly crystallized (the inset in Figure 3b), suggesting the crystallization effect induced by the hydrothermal treatment. The crystal sizes calculated are about 23.5 nm for FWO/C-0.5 and 41.2 nm for FWO/C-5. The nanosized particles are conducive to improving the electrochemical performance of FWO as anode materials for

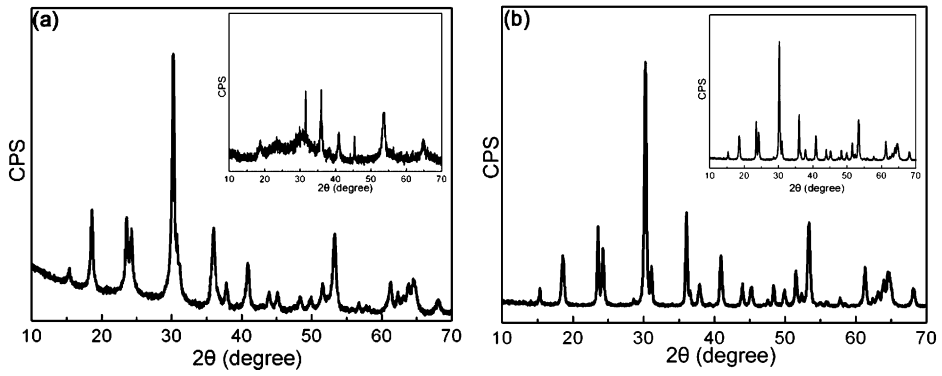

Figure 3. XRD patterns of FWO/C-0.5 (a) and FWO/C-5 (b). The insets are the corresponding XRD patterns of FWO-0.5 and FWO-5.

LIBs.[20−23] When the hydrothermal time is over 5 h, the XRD patterns are very similar to those for FWO-5 and FWO/C-5, implying that the structure changes no longer; however, the particle size increases with prolonging hydrothermal time. From the TEM image of FWO/C-10 displayed in Figure S4 in the Supporting Information, most of the particles are bigger than 50 nm.

The morphology of the hydrothermal products was also examined by TEM, as shown in Figure 4. From Figure 4a, the

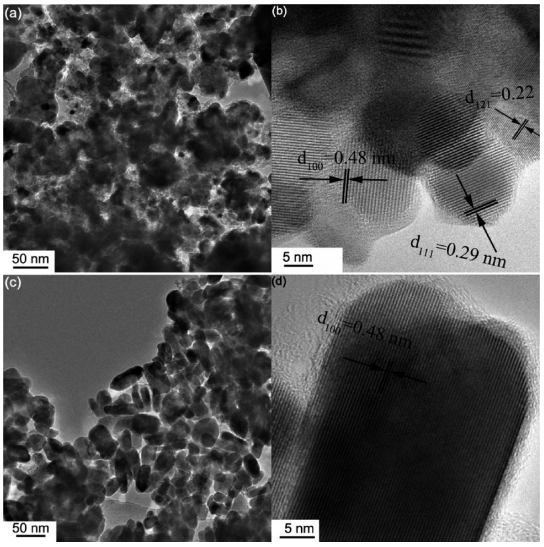

Figure 4. TEM images of FWO/C-0.5 (a, b) and FWO/C-5 (c, d).

particle size of FWO/C-0.5 ranges from several nanometers to 50 nm, smaller than that of FWO/C-5 owing to the shorter hydrothermal duration. The carbon layer on FWO/C-0.5 (1.1 nm or so) is thinner than that on FWO/C-5 (about 1.6 nm). Because the weight of FWO and the volume of pyrrole for the two samples are the same, the thinner carbon layer for FWO/C-0.5 is mainly associated with the larger specific surface area of the smaller particles. As a confirmation, nitrogen adsorption/desorption isotherms of the two samples were measured (Figure S1 in the Supporting Information). The type II character of the isotherms indicates that the carbon-coated FWO is not a porous material. The specific surface areas calculated are 35.8 $m^2\ g^{-1}$ for FWO/C-0.5, and 23.1 $m^2\ g^{-1}$ for FWO/C-5. The larger surface area of FWO/C-0.5 than FWO/C-5 also demonstrates the smaller particle size of FWO/C-0.5 than FWO/C-5.

The clear lattice fringes in Figure 4b,d that can be indexed to different planes of FWO confirm the well-crystallized structure. For FWO/C-5, the nanocrystals reveal a uniform size of 40 nm or so, implying a tendency of grain growth with prolonging hydrothermal time.

The carbon-coated samples were also characterized by Raman spectroscopy, as shown in Figure 5a. The broad peak located at about 1309 cm^{-1} represents the D band (disordered carbon), and the one around 1589 cm^{-1} is the G band (graphitic carbon).[24] The intensity ratio of the two peaks (I_D/I_G) reveals the disordered degree of carbon materials. The ratio is approximately 1.0 for FWO/C-0.5 and FWO/C-5, demonstrating the low graphitization degree of the carbon coating.

TGA was utilized to determine the carbon content in the carbon-coated samples, as displayed in Figure 5b. The weight loss below 300 °C is due to the evaporation of water absorbed on the surface of the samples, and the rapid weight loss around 400 °C resulted from the oxidation of carbon. The weight loss is 9.9 wt % for FWO/C-0.5 and 6.0 wt % for FWO/C-5. These results are consistent with those acquired from the elemental analyzer (Table S1 in the Supporting Information).

3.2.2. Electrochemical Performance. The charge/discharge curves for selected cycles of FWO/C-5 are shown in Figure 6a. During the first discharging, the voltage falls rapidly to about 1.1 V, followed by a continuous decrease with a turning point around 0.55 V, which is the characteristic behavior of the reduction of W^{6+} and Fe^{2+} to W(0) and Fe(0).[10,25] The difference between the discharge curve of the first cycle with those of the subsequent cycles may result from the irreversible destruction of FWO crystals.[21,26] During charging, the voltage curve reveals a plateau around 1.5 V, in good agreement with that reported in the literature.[11]

From the second cycle, the sloped voltage curve contains several overlapped plateaus around 1.6 V during discharging, and at about 1.0 and 1.4 V during charging. These plateaus indicate that the conversion reaction involves multiple steps due to the reduction of W^{6+} and Fe^{2+} to W(0) and Fe(0), just like the mechanism proposed in the literature.[11]

$$FeWO_4 + 8Li^+ + 8e^- \leftrightarrow Fe + W + 4Li_2O$$

It can also be found that both the charge curves and the discharge ones almost coincide mutually after the second cycle, indicative of the excellent cyclability of the FWO/C anodes. The charge/discharge curves of FWO/C-0.5 are analogous to those of FWO/C-5, implying that similar electrochemical reactions occur in the FWO/C-0.5 anodes.

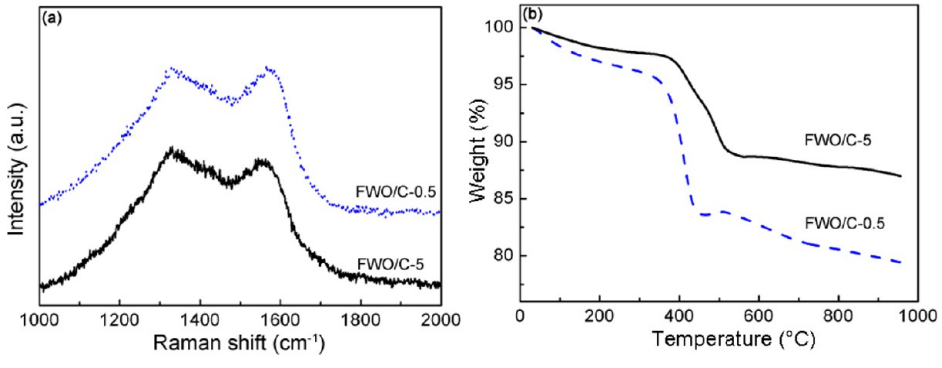

Figure 5. (a) Raman spectra and (b) TGA curves of FWO/C-0.5 and FWO/C-5.

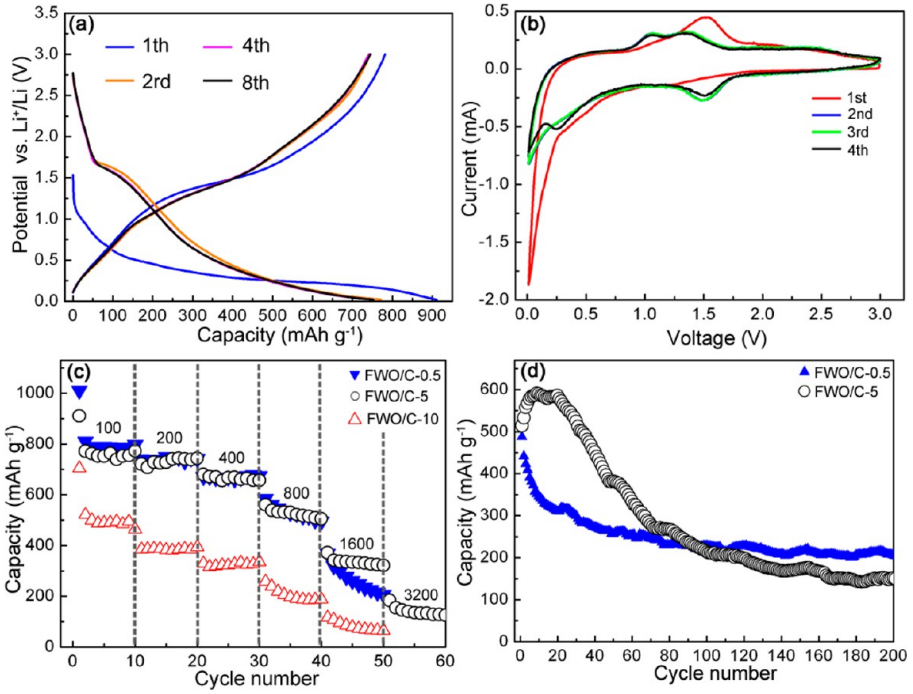

Figure 6. (a) Charge/discharge curves of FWO/C-5. (b) Cyclic voltammograms of FWO/C-0.5 for the first four cycles. (c) Rate capabilities of FWO/C-0.5, FWO/C-5, and FWO/C-10. (d) Long-term cycling performance of FWO/C-0.5 and FWO/C-5 cycled at a current density of 800 mA g^{-1}.

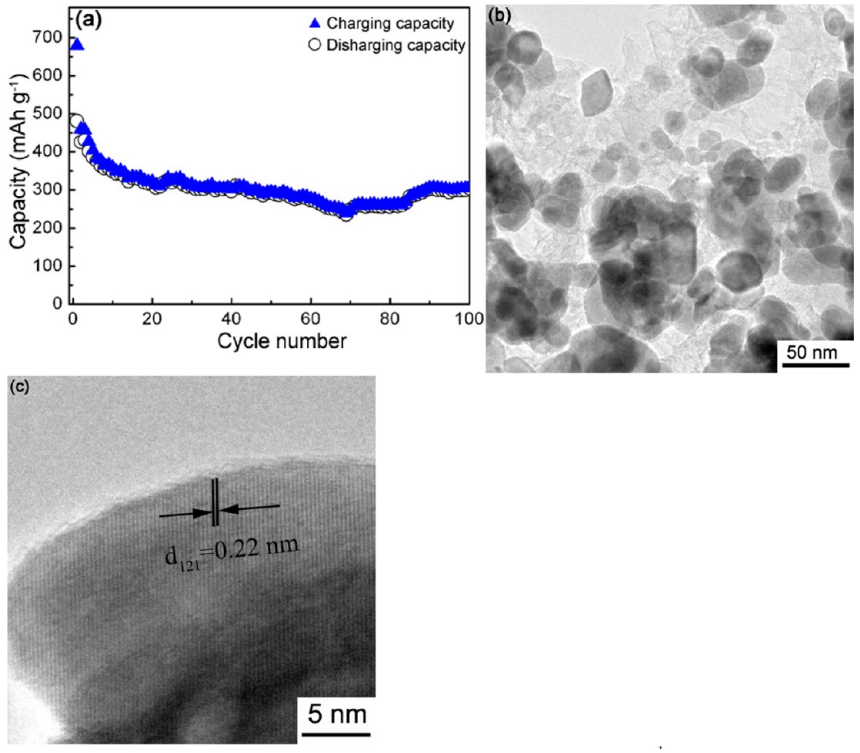

Figure 7. Cycling performance at a current density of 100 mA g^{-1} (a). TEM images of FWO/GC-5 (b, c).

The cyclic voltammograms of FWO/C-0.5 were measured at a scan rate of 0.1 mV s^{-1}, as shown in Figure 6b. The voltammogram for the first cycle is different from those for the other cycles due to the irreversible destruction of FWO crystals and the formation of SEI films. An anodic peak at about 1.5 V occurs from the second cycle. Two pairs of peaks around 1.0 and 1.4 V during charging and ~1.6 and 0.5 V during discharging also indicate the multi-step electrochemical reactions involved in the $FeWO_4$ anode.[11] These results are consistent with those observed in Figure 6a.

Rate performance is important for electrode materials, especially for large-scale lithium storage devices. The rate capabilities of FWO/C-0.5, FWO/C-5, and FWO/C-10 are displayed in Figure 6c. When the current density is not higher

than 800 mA g^{-1}, the former two samples exhibit almost the same capacities at each identical density. Even at high current densities of 1600 and 3200 mA g^{-1}, FWO/C-5 could deliver reversible capacities of 342.2 and 184.0 mAh g^{-1}, superior to those of FWO/C-0.5. However, the rate performance of FWO/C-10 is poor due to the larger particle size. The capacities at various rates for the carbon-coated products are tabulated in Table 1. It is obvious that the hydrothermal treatment for 0.5−5 h is beneficial for the rate capabilities, within which FWO/C-5 exhibits better performance at high rates. This could also be supported by other test results revealed in Figure S3 of the Supporting Information, from which the discharge capacities also conform to the same variation tendency.

Long-term cycling performance was recorded at a current density of 800 mA g^{-1}, as displayed in Figure 6d. Though the reversible capacities of FWO/C-5 during the initial 50 cycles are higher than those of FWO/C-0.5, the capacities of FWO/C-0.5 are relatively stable. After 200 cycles, the reversible capacities are 151.9 mAh g^{-1} for FWO/C-5 and 205.9 mAh g^{-1} for FWO/C-0.5. The crystallinity and crystal size of FWO increase with prolonging hydrothermal time. Compared with the reversible capacity and rate performance of FWO/C-0, FWO/C-0.5 and FWO/C-5 exhibit improved electrochemical performance partially because of the high crystallinity that resulted from the hydrothermal treatment. However, the performance decreases (Figure 6c) when the hydrothermal time is over 10 h due to the bigger particle size (Figure S4, Supporting Information), because the smaller particles are favorable to shorten the diffusion path of Li ions.[20,21] Although FWO/C-0.5 exhibits higher performance than FWO/C-5 at the current densities below 800 mA g^{-1}, the rate performance of FWO/C-5 at the current densities higher than 1600 mA g^{-1} is slightly superior to that of FWO/C-0.5, demonstrating that appropriate particle size is beneficial for achieving high electrochemical performance of transition-metal oxides.[20,21] In comparison with the result in the literature,[11] the FWO/C anodes exhibit remarkably enhanced electrochemical performance owing to the uniformly formed carbon coating. Similar improvement in electrochemical performance resulting from the carbon coating was also observed in the metal tungstates of $ZnWO_4$[9] and $CaWO_4$.[10]

3.2.3. Enhancement of Electrochemical Performance by Coating N-Carbon. Carbon coating doped with nitrogen has been demonstrated to be an effective way to improve the electrochemical performance of electrodes,[12,13] because nitrogen-doping could increase the charge carriers in carbon materials,[27] thus contributing to improving the electronic conductivity.[28] The formation of the N-carbon coating in the presence of pyrrole has been reported in our previous work.[13]

As a comparison, the electrochemical performance of FWO/GC-5 was also measured, as exhibited in Figure 7a. After cycling 100 times at 100 mA g^{-1}, FWO/GC-5 displays a capacity of 348.0 mAh g^{-1}, much lower than those of FWO/C-0 and FWO/C-5, further confirming the beneficial effect of N-carbon coating on the electrochemical performance of FWO. From the TEM images of FWO/GC-5 shown in Figure 7b, besides the FWO nanoparticles, some free carbon could also be observed in the sample, and the corresponding HRTEM image (Figure 7c) reveals the thin and uneven carbon coating on the FWO surface, further demonstrating that, under the same conditions, using pyrrole as the carbon source to coat FWO is advantageous over using glucose.

To understand the effect of the N-carbon coating on the electrochemical performance, the electrochemical impedance spectra of FWO/C-0, FWO/C-0.5, FWO/C-5, and FWO/GC-5 in the charge state are shown in Figure 8. The semicircle in

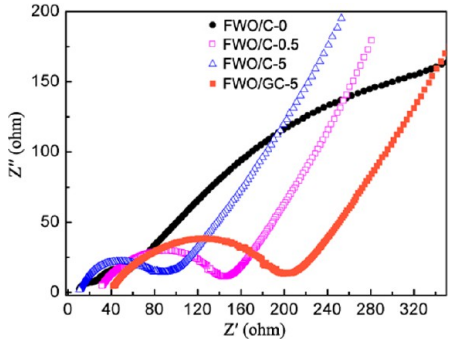

Figure 8. Nyquist plots of the FWO/C-0, FWO/C-0.5, FWO/C-5, and FWO/GC-5 cells.

the high-frequency range represents the impedance from the surface film (R_{sf}) and charge transfer (R_{ct}), and the two parts could not be distinguished from the plots. The impedance values of ∼140 Ω for FWO/C-0.5 and ∼90 Ω for FWO/C-5 could well support the improved cycling performance of the two samples. In the low-frequency region, compared with the straight sloping lines for FWO/C-0.5 and FWO/C-5, the inclined line with a small gradient for FWO/C-0 demonstrates a high Warburg impedance, which will result in the capacity fading during cycling.[29] Compared to FWO/C-0.5 and FWO/C-5, FWO/GC-5 exhibits a larger $R_{(sf+ct)}$ (∼200 Ω), which is responsible for the poor electrochemical performance. The effect of different carbon sources on the electrochemical performance further demonstrates the advantages of the N-cabon derived from pyrrole. Despite a lower $R_{(sf+ct)}$ for FWO/C-0 (about 60 Ω), the high Warburg impedance reflects the slow reaction kinetics of Li ions in the sample. The low $R_{(sf+ct)}$ and Warburg impedance for the hydrothermal products are demonstrative of the better conductivity and fast Li-ion kinetics, which are favorable to remarkably enhance the electrochemical performance of the FWO/C anodes, just like what is revealed in Figure 6 and Table 1.

As stated above, the excellent electrochemical performance of FWO/C is related to the following factors: (1) The hydrothermal treatment for short duration could refine the grain size of FWO, while the nanocrystals are favorable for increasing the contact area between electrode and electrolyte and for shortening the Li-ion transfer pathway. (2) The combination of the good electron transport performance of FWO,[8] and WO_3,[30] with the N-carbon coating (which could improve the electronic conductivity between nanoparticles) contributes to enhancing the overall conductivity of the FWO/C anodes (Figure 8). (3) The carbon coating could efficiently buffer the drastic volume change during Li-ion insertion/extraction. (4) The coexistence of heterogeneous elements of W and Fe or their oxides in the carbon shells could act as dispersants mutually to inhibit their assembly during charging/discharging, which might explain why the performance of FWO/C is superior to that of WO_3 and FWO reported in the literature.[11,30−35]

4. CONCLUSION

Carbon-coated FWO was obtained by hydrothermally processing FWO at 180 °C, followed by coating carbon using pyrrole as a precursor. The FWO/C as anode materials exhibits excellent rate capabilities and long-term cycling performance even when cycled at a current density of 800 mA g^{-1}. The impressive electrochemical performance suggests the great potential of the FWO/C anodes for energy storage and application in hybrid vehicles.

■ ASSOCIATED CONTENT

Ⓢ Supporting Information

Nitrogen adsorption/desorption isotherms, table of the C and N contents in the samples, Raman spectrum, TGA curve, rate capabilities, and TEM image. This material is available free of charge via the Internet at http://pubs.acs.org.

■ AUTHOR INFORMATION

Corresponding Author

*E-mail: byj97@126.com (Y.-J.B.), fan@sdu.edu.cn (R.-H.F.). Tel/Fax: +8653188392315 (R.-H.F.).

Notes

The authors declare no competing financial interest.

■ ACKNOWLEDGMENTS

This work was supported by the Independent Innovation Foundation of Shandong University, IIFSDU (2012ZD004), the Open Project from State Key Laboratory of Crystal Materials (KF1105), the National Natural Science Foundation of China (Nos. 50972076 and 51172131), and the Shandong Provincial Natural Science Foundation, China (Y2008F26 and Y2008F40).

■ REFERENCES

(1) Li, G. S.; Zhang, D. Q.; Yu, J.; Leung, M. *Environ. Sci. Technol.* **2010**, *44*, 4276−4281.
(2) Gould, D. M.; Griffith, W. P.; Spiro, M. *J. Mol. Catal. A: Chem.* **2001**, *175*, 289−291.
(3) Zhou, Y. X.; Yao, H. B.; Zhang, Q.; Gong, J. Y.; Liu, S. J.; Yu, S. H. *Inorg. Chem.* **2009**, *48*, 1082−1090.
(4) Gao, Y.; Zhao, J. Z.; Zhu, Y. C.; Ma, S. S.; Su, X. D.; Wang, Z. C. *Mater. Lett.* **2006**, *60*, 3903−3905.
(5) Blasse, L. *Chem. Phys. Lett.* **1990**, *173*, 409−411.
(6) Lou, Z.; Cocivera, M. *Mater. Res. Bull.* **2002**, *37*, 1573−1582.
(7) Nikl, M.; Bohacek, P.; Mihokova, E.; Kobayashi, M.; Ishii, M.; Usuki, Y.; Babin, V.; Stolovich, A.; Zazubovich, S.; Bacci, M. *J. Lumin.* **2000**, *87−89*, 1136−1139.
(8) Schmidbauer, E.; Schanz, U.; Yu, F. J. *J. Phys.: Condens. Matter* **1991**, *3*, 5341−5352.
(9) Shim, H. W.; Lim, A. H.; Lee, G. H.; Jung, H. C.; Kim, D. W. *Nanoscale Res. Lett.* **2012**, *7*, 9.
(10) Sharma, N.; Subba Rao, G. V.; Chowdari, B. V. R. *Electrochim. Acta* **2005**, *50*, 5305−5312.
(11) Shim, H. W.; Cho, I. S.; Hong, K. S.; Cho, W., II.; Kim, D. W. *Nanotechnology* **2010**, *21*, 465602−465608.
(12) Lei, C.; Han, F.; Li, D.; Li, W. C.; Sun, Q.; Zhang, X. Q.; Lu, A. H. *Nanoscale* **2013**, *5*, 1168−1175.
(13) Gong, C.; Bai, Y. J.; Qi, Y. X.; Lun, N.; Feng, J. *Electrochim. Acta* **2013**, *90*, 119−127.
(14) Lu, K. *Adv. Mater.* **1999**, *11*, 1127−1128.
(15) Cherian, C. T.; Sundaramurthy, J.; Kalaivani, M.; Ragupathy, P.; Kumar, P. S.; Thavasi, V.; Reddy, M. V.; Sow, C. H.; Mhaisalkar, S. G.; Ramakrishna, S.; Chowdari, B. V. R. *J. Mater. Chem.* **2012**, *22*, 12198−12204.
(16) Zhou, G.; Wang, D. W.; Li, F.; Zhang, L.; Li, N.; Wu, Z. S.; Wen, L.; Lu, G. Q.; Cheng, H. M. *Chem. Mater.* **2010**, *22*, 5306−5313.
(17) Wang, Z. Y.; Luan, D. Y.; Madhavi, S.; Hu, Y.; Lou, X. W. *Energy Environ. Sci.* **2012**, *5*, 5252−5256.
(18) Zhang, W. M.; Wu, X. L.; Hu, J. S.; Guo, Y. G.; Wan, L. J. *Adv. Funct. Mater.* **2008**, *18*, 3941−3946.
(19) Yu, Y.; Gu, L.; Wang, C. L.; Dhanabalan, A.; van Aken, P. A.; Maier, J. *Angew. Chem., Int. Ed.* **2009**, *48*, 6485−6489.
(20) Aricò, A. S.; Bruce, P.; Scrosati, B.; Tarascon, J. M.; Van Schalkwijk, W. *Nat. Mater.* **2005**, *4*, 366−377.
(21) Poizot, P.; Laruelle, S.; Grugeon, S.; Dupon, L.; Tarascon, J. M. *Nature* **2000**, *407*, 496−499.
(22) Song, M. K.; Park, S.; Alamgir, F. M.; Cho, J.; Liu, M. L. *Mater. Sci. Eng., R* **2011**, *72*, 203−252.
(23) Ji, L. W.; Lin, Z.; Alcoutlabi, M.; Zhang, X. W. *Energy Environ. Sci.* **2011**, *4*, 2682−2699.
(24) Robertson, J. *Mater. Sci. Eng., R* **2002**, *37*, 129−281.
(25) Reddy, M. V.; Yu, T.; Sow, C. H.; Shen, Z. X.; Lim, C. T.; Rao, G. V. S.; Chowdari, B. V. R. *Adv. Funct. Mater.* **2007**, *17*, 2792−2799.
(26) Kim, D. W.; Ko, Y. D.; Park, J. G.; Kim, B. K. *Angew. Chem., Int. Ed.* **2007**, *46*, 6654−6657.
(27) Xiao, K.; Liu, Y. Q.; Hu, P. A.; Yu, G.; Sun, Y. M.; Zhu, D. B. *J. Am. Chem. Soc.* **2005**, *127*, 8614−8617.
(28) Choi, Y. M.; Lee, D. S.; Czerw, R.; Chiu, P. W.; Grobert, N.; Terrones, M.; Reyes−Reyes, M.; Terrones, H.; Charlier, J. C.; Ajayan, P. M.; Roth, S.; Carroll, D. L.; Park, Y. W. *Nano Lett.* **2003**, *3*, 839−842.
(29) Teh, P. F.; Sharma, Y.; Pramana, S. S.; Srinivasan, M. *J. Mater. Chem.* **2011**, *21*, 14999−15008.
(30) Yoon, S. H.; Jo, C. S.; Noh, S. Y.; Lee, C. W.; Song, J. H.; Lee, J. *Phys. Chem. Chem. Phys.* **2011**, *13*, 11060−11066.
(31) Yang, J. Q.; Jiao, L. F.; Zhao, Q. Q.; Wang, Q. H.; Gao, H. Y.; Huan, Q. N.; Zheng, W. J.; Wang, Y. J.; Yuan, H. T. *J. Mater. Chem.* **2012**, *22*, 3699−3701.
(32) Gu, Z. J.; Li, H. Q.; Zhai, T. Y.; Yang, W. S.; Xia, Y. Y.; Ma, Y.; Yao, J. N. *J. Solid State Chem.* **2007**, *180*, 98−105.
(33) Huang, K.; Pan, Q. T.; Yang, F.; Ni, S. B.; Wei, X. C.; He, D. Y. *J. Phys. D: Appl. Phys.* **2008**, *41*, 155417−155421.
(34) Yu, A. S.; Kumagai, N.; Liu, Z. L.; Lee, J. Y. *J. Solid State Electrochem.* **1998**, *2*, 394−400.
(35) Kumagai, N.; Kumagai, N.; Umetzu, Y.; Tanno, K.; Pereira-Ramos, J. P. *Solid State Ionics* **1996**, *86−88*, 1443−1449.